

Proton-conductivity anisotropy in CsHSO_4 and CsDSO_4 crystals and its response to hydrostatic pressure

V. V. Sinitsyn, E. G. Ponyatovskii, A. I. Baranov,¹⁾ A. V. Tregubchenko,¹⁾ and L. A. Shuvalov¹⁾

Institute of Solid State Physics, USSR Academy of Sciences
(Submitted 12 April 1991)

Zh. Eksp. Teor. Fiz. **100**, 693–706 (August 1991)

The temperature (270–480 K) and baric (up to 2.0 GPa) dependences of the proton conductivities of CsHSO_4 and CsDSO_4 crystals were investigated in different crystallographic directions. The orientation of the conductivity tensor and the temperature dependence of its components were determined in the low ($\sigma < 10^{-7} \Omega^{-1} \cdot \text{cm}^{-1}$) and super-ionic ($\sigma \gg 10^{-3} \Omega^{-1} \cdot \text{cm}^{-1}$) phases. The conductivity itself and the parameters that determine it (the enthalpy and the pre-exponential factor in the Arrhenius law), were found to be anisotropic. Estimates show that the activation volumes of the proton conductivity are anisotropic and more sensitive to weak structural changes than the activation enthalpy and the pre-exponential factor. The activation volume ranges from –1.6 to 2.0 cm^3/mol , depending on the phase and direction.

1. INTRODUCTION

Notwithstanding the many investigations of proton diffusion and proton conductivity in crystals with hydrogen bonds (see, e.g., Refs. 1–3), the general laws governing the proton transport mechanism still remain unclear.

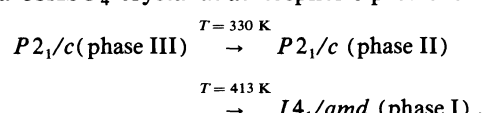
The reason, on the one hand, is that the densities of the mobile protons and proton vacancies in most crystals are insufficient to yield information on their migration paths by direct experimental methods (neutron investigations, NMR, and optical spectroscopy). On the other hand, proton transport in such compounds is governed by specific features of the hydrogen bond which has not yet been fully studied.

Research into the connection between the dynamic parameters indicative of the proton transport, on the one hand, and into the hydrogen-bond thermodynamic parameters which are connected in turn with the geometry of these bonds and with the coordination of the surrounding atom, on the other, is therefore of particular interest. Investigations of the influence of pressure are in this respect the most informative. Promising objects for such research are compounds with structural (positional) disorder of the proton, similar to that observed for silver ions in the super-ionic phase of the AgI crystal. Particular attention attaches here to crystals in which the symmetry group of the ordered phase (with low proton conductivity) is a symmetry subgroup of the disordered super-ionic phase. The total number of crystallographic (not necessarily structurally equivalent) positions in which the protons can be localized to form hydrogen bonds in phases with different conductivity remains unchanged in this case, and the phases differ only in the probability that protons can occupy these positions. Therefore the results of investigations of each of the phases supplement one another and yield a more complete picture of the features of the structural mechanism of the conductivity. No less important for a clarification of this mechanism are also investigations of the conductivity anisotropy and its connection with the geometric features of the network of hydrogen bonds.

These investigations can be realized on crystals of alkaline hydrosulfates (hydroxelenates). It was established earlier^{3–7} that high-temperature super-ionic phases are realized in these crystals, and their hydrogen-bond geometry differs

from that of low-temperature low-conductivity phases.

The following sequence of phase transitions takes place in a CsHSO_4 crystal at atmospheric pressure:^{4–8}



The III–II phase transition is of the reconstructive type and is poorly reversible, while the II–I phase transition is superionic and simultaneously not properly ferroelastic.⁷ Its symmetry description on the basis of the Landau theory is given in Ref. 9. In the low-conductivity phase III ($\sigma < 10^{-7} \Omega^{-1} \cdot \text{cm}^{-1}$) the hydrogen bonds join the SO_4^{2-} groups into chains, which are rotated in the phase transition through 45° in the (100) plane.^{5,6} The paraelectric phase I is super-ionic with a proton conductivity $\sigma \gg 10^{-3} \Omega^{-1} \cdot \text{cm}^{-1}$ (Refs. 4 and 8). The results of x-ray-structure and neutron-diffraction investigations^{7,8} as well as a symmetry analysis show that in phase I the number of structurally and hence physically equivalent positions in which the protons can form a hydrogen bond exceeds by several times the number of protons, and according to NMR data¹¹ the proton lifetime in these positions is $\sim 10^{-8} \text{ s}$. It is seen from the aggregate of these data that in phase I the protons form a dynamically disordered hydrogen-bond network responsible for the high conductivity.³ When H is replaced by D the temperature of the super-ionic II–I transition is slightly lowered ($\approx 3^\circ$) and phase II remains stable down to liquid helium temperatures.

We have investigated the temperature and baric dependences of the proton conductivity for various orientations of the crystals CsHSO_4 (CHS) and CsDSO_4 (CDS). We determined in all three phases the orientation of the conductivity tensor relative to the crystallographic axes and the temperature dependence of its principal components.

2. MEASUREMENT PROCEDURE AND SAMPLES

We measured the conductivity of $5 \times 5 \times 1 \text{ mm}$ single-crystal samples oriented along the crystallographic axes, and also of powders pressed into pellets. The electrodes used were “Degussa” silver paste or metal (gold, silver) powders thermally sputtered in vacuum. To exclude surface conduc-

tivity, which can be comparable with bulk conductivity in low-temperature phases,¹² the single-crystal samples were measured also in setups with “guard rings.”

At atmospheric pressure the bulk conductivity was calculated from the frequency dependence of the complex admittance. The measurements were made with an “Ando Electric” TP-10C *ac* bridge in the frequency range 30 Hz–1 MHz and with a VM-431 bridge at 1–200 MHz. The sample was measured in an argon atmosphere to prevent absorption of water. This practice was important also for measurements of deuterated samples in the super-ionic phase, where the rapid diffusion in an air atmosphere caused an isotopic (D→H) exchange with the ambient during the measurements.¹³

The conductivity in a high-pressure chamber was measured at a fixed frequency chosen so that the measured conductivity hardly differed from the static bulk conductivity determined from the frequency dependence of the admittance. Measurements were made in the low-conducting phases under pressure at 1 kHz with an E7-8 bridge, and in the super-ionic phases under pressures up to 20 GPa at 1 MHz with a E7-12 bridge, at temperatures 30–550 K. The pressure-transmitting medium was silicone oil. The sample temperature was measured with a chromel-alumel thermocouple (accuracy $\pm 1^\circ$), and the pressure with a manganine sensor (accuracy ± 0.02 GPa).

3. IONIC-CONDUCTIVITY TENSOR

The anisotropy of the ion (proton) transport in crystals reflects the geometric features of the crystal lattices. In the macroscopic approach the onset of anisotropy can be explained using atomistic hopping-conduction models. Following Flynn,¹⁴ we consider a crystal containing s types of different interstitial positions (with multiplicity g_q , where $q = 1, \dots, s$) forming a Bravais lattice or having symmetry no lower than tetragonal. The charge flow from positions of type q into the nearest position of type k can be expressed as

$$\mathbf{J}^{qk} = eZn_0c_q(1 - c_k)\mathbf{v}^{qk} = eZn_0c_q(1 - c_k)\nu^{qk}\mathbf{l}^{qk}, \quad (1)$$

where \mathbf{v}^{qk} , ν^{qk} and \mathbf{l}^{qk} are the velocity, the hopping frequency, and the length, which describe the motion of the ion from position q to k ; n_0 is the atomic density of the migrating ions; eZ is their charge; $1 - c_k$ is the probability that the position k is free; c_q is the probability of finding the ion in position q .

Let the number of nearest positions into which the ion goes from a position q be N_q . Then we obtain the ion flux J by summing over all the positions closest to q and over all s types of positions contained in the crystal:

$$\mathbf{j} = \sum_{q=1}^s \sum_{k=1}^{N_q} eZn_0c_q(1 - c_k)\nu^{qk}\mathbf{l}^{qk}. \quad (2)$$

At thermodynamic equilibrium the total current in the crystal is zero if there is no external field. A static electric field \mathbf{E} alters the hopping frequency ν^{qk} and produces a non-zero current \mathbf{J} :

$$\mathbf{j} = \sum_{q=1}^s \sum_{k=1}^{N_q} eZn_0c_q(1 - c_k)\delta\nu^{qk}\mathbf{l}^{qk} = \hat{\sigma}\mathbf{E}, \quad (3)$$

where $\delta\nu^{qk}$ is the change of the frequency of hopping between positions q and k in the presence of the field \mathbf{E} and its ab-

sence; $\hat{\sigma}$ is the ionic conductivity tensor.

If the ion hopping is thermally activated, we have

$$\nu^{qk} = v_0^{qk} \exp(-\Phi_m^{qk}/k_B T), \quad (4)$$

where v_0^{qk} is the oscillation frequency of a mobile atom in position q in the direction of the vector \mathbf{l}^{qk} ; Φ_m^{qk} is the change of the thermodynamic potential of the crystal when the atom goes from position q into k . In this case

$$\begin{aligned} \delta\nu^{qk} &= v_0^{qk} \exp\left(-\frac{\Phi_m^{qk} - 1/2eZE\mathbf{l}^{qk}}{k_B T}\right) - v_0^{qk} \exp\left(-\frac{\Phi_m^{qk}}{k_B T}\right) \\ &= v_0^{qk} \exp\left(-\frac{\Phi_m^{qk}}{k_B T}\right) \left[\exp\left(\frac{eZE\mathbf{l}^{qk}}{2k_B T}\right) - 1 \right] \\ &\approx v_0^{qk} \left(\frac{eZE\mathbf{l}^{qk}}{2k_B T} \right) \exp\left(-\frac{\Phi_m^{qk}}{k_B T}\right). \end{aligned} \quad (5)$$

Taking (5) and (3) into account we obtain for the components of the conductivity tensor σ_{ij}

$$\sigma_{ij} = -\frac{1}{2} \frac{(eZ)^2 n_0}{k_B T} \left[\sum_{q=1}^s c_q \sum_{k=1}^{N_q} (1 - c_k) l_i^{qk} l_j^{qk} v_0^{qk} \exp\left(-\frac{\Phi_m^{qk}}{k_B T}\right) \right]. \quad (6)$$

The conductivity measured in an arbitrary direction \mathbf{n} , expressed in terms of the principal component of the tensor (6), is

$$\sigma_{ij} = \sigma_{11} \cos \gamma_1 + \sigma_{22} \cos \gamma_2 + \sigma_{33} \cos \gamma_3, \quad (7)$$

where σ_{ii} are the components of the conductivity tensor referred to the principal axes, $\cos \gamma_i$ being the direction cosines of \mathbf{n} in the principal coordinate frame.

The values of $|\mathbf{l}^{qk}|$, v_0^{qk} and Φ_m^{qk} can differ for different index pairs q and k , so that in general the temperature dependence of $\sigma(\mathbf{n}, T)$ is described by a sum of exponentials rather than by the Arrhenius law. Numerous experimental data indicate nonetheless that the Arrhenius law holds for many ionic conductors in rather wide temperature ranges. This justifies the use in our results, for different directions of \mathbf{n} , of the approximation

$$\sigma(\mathbf{n}, T) = \frac{A_0(\mathbf{n})}{T} \exp\left(-\frac{\Phi^a(\mathbf{n})}{k_B T}\right), \quad (8)$$

where $A_0(\mathbf{n})$ and $\Phi^a(\mathbf{n})$ are effective parameters that depend on the direction.

For $\Phi^a(\mathbf{n})$ in the form

$$\Phi^a(\mathbf{n}) = E^a(\mathbf{n}) - TS^a(\mathbf{n}) + pV^a(\mathbf{n}) \quad (9)$$

we have

$$\begin{aligned} \sigma(\mathbf{n}, T) &= \frac{A(\mathbf{n})}{T} \exp\left(-\frac{E^a(\mathbf{n}) + pV^a(\mathbf{n})}{k_B T}\right) \\ &= \frac{A(\mathbf{n})}{T} \exp\left(-\frac{H^a(\mathbf{n})}{k_B T}\right), \end{aligned} \quad (10)$$

where $\Phi^a(\mathbf{n})$, $E^a(\mathbf{n})$, $S^a(\mathbf{n})$, $H^a(\mathbf{n})$, and $V^a(\mathbf{n})$ are the effective thermodynamic potential, activation energy, entropy, activation enthalpy, and activation volume. In contrast to the isotropic case, they are functions of the directions \mathbf{n} , and $A(\mathbf{n}) = A_0(\mathbf{n}) \exp(S^a(\mathbf{n})/k_B)$ is the effective value of the pre-exponential factor, which likewise depends on direction.

We express, by analogy, $A_0(\mathbf{n})$ in terms of the effective values of the oscillation frequency $\nu_0(\mathbf{n})$ and the hopping distance $l(\mathbf{n})$ in the \mathbf{n} direction:

$$A_0(\mathbf{n}) = \frac{1}{2} \frac{n_0(eZ)^2}{k_B} \nu_0(\mathbf{n}) l^2(\mathbf{n}). \quad (11)$$

4. PROTON CONDUCTIVITY AT ATMOSPHERIC PRESSURE

Figure 1 shows the temperature dependence of the conductivities in phases III and II of CHS and CDS crystals, measured in various crystallographic directions. The conductivity in these phases has evidently appreciable anisotropy. In phase III, in particular, $\sigma(\mathbf{b})$ and $\sigma(\mathbf{c}^*)$, differ by two orders of magnitude. On the other hand, the appreciable difference between the corresponding conductivity components in the isostructural II phases of the CHS and CDS crystals is conspicuous. Note in this connection that the CHS samples had the same orientation as the crystallographic axes of phase III, which differs from that of phase II. Allowance for this difference, however, does not account completely for the observed difference between the conductivities of CHS and CDS in phase II.

Observation of the CHS III-II phase transition in polarized light shows that this transition produces macroscopic phase-II blocks with different crystallographic orientations. In addition, phase-III regions are preserved in a wide temperature interval above T_{III-II} . To verify that these are the main causes of the conductivity differences between the II phases of CHS and CDS crystals, we measured the conductivities of pellets pressed from CHS and CDS powders. These measurements show that in this case there is actually no difference between the temperature dependences of the II phases of CHS and CDS, which are close to the corresponding dependences shown in Fig. 1 for single-crystal phase-II CHS samples. Hence, we shall use in the analysis of phase-II conductivity only the data obtained for deuterated crystals.

In accordance with the symmetry of phases III and II

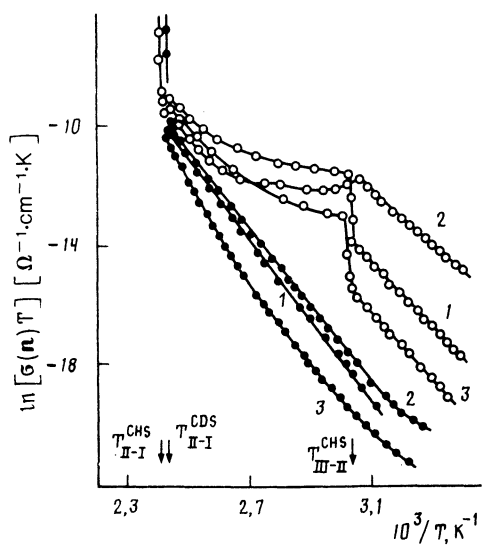


FIG. 1. Temperature dependence of proton conductivity $\sigma(\mathbf{n})$ (\circ — CsHSO_4 , \bullet — CsDSO_4) for various crystallographic directions \mathbf{n} : 1— \mathbf{c}^* ; 2— \mathbf{b} ; 3— \mathbf{a}^* . T_{III-II}^{CHS} —temperature of III-II phase transition in CsHSO_4 crystal; CsHSO_4 ; T_{II-I}^{CHS} and T_{II-I}^{CDS} —temperatures of superionic transitions in CsHSO_4 and CsDSO_4 crystals.

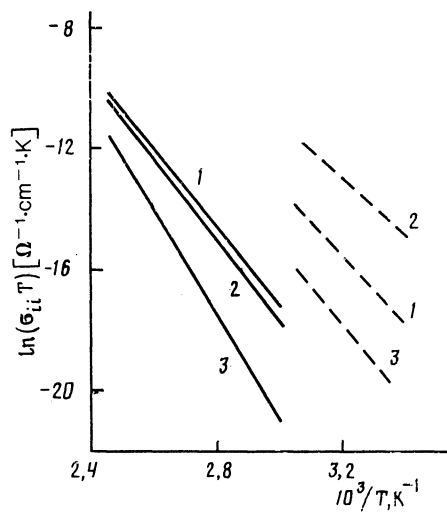


FIG. 2. Temperature dependence of principal components of conductivity tensor in the phases III (dashed) and II (solid): 1— σ_{11} ; 2— σ_{22} ; 3— σ_{33} .

(point group $2/m$), one of the principal axes of the conductivity tensor coincides with the [010] direction. To determine the other two principal axes it suffices therefore to perform the measurements on three samples whose normals lie in the (010) plane. The temperature dependence of the principal components of the tensor, calculated from such measurements, is shown in Fig. 2. In the (010) plane the principal axes of the conductivity tensor σ_{ij} were found to be close to the crystallographic axes \mathbf{a}^* and \mathbf{c}^* . When the temperature is raised the angle γ_1 between the tensor axis \mathbf{x}^* and the \mathbf{a}^* direction changes insignificantly, by approximately 3° .

The temperature dependence of $\ln[\sigma(\mathbf{n})T] = f(1/T)$ for the investigated orientations is also well approximated by Eq. (10), and the anisotropy of the conductivity reflects the symmetry of this phase (point group $4/mmm$), namely, $\sigma(\mathbf{a})$ and $\sigma(\mathbf{b})$ agree to within the limits of the experimental error ($\sigma(\mathbf{a}) = \sigma(\mathbf{b}) = \sigma_\perp$) and differ somewhat from $\sigma(\mathbf{c}^*) = \sigma_\parallel$ (Fig. 2). Actually, however, the isotropic conductivity can be larger in this phase, since the II-I phase transition (and also the III-II transition in CHS) is accompanied by subdivision of the sample into blocks whose misorientation can reach $\sim 10^\circ$ (Ref. 15), so that the conductivity averages out over the different directions. It is evident from Table I, which shows the values of H^a and A_a in all three phases, that both the pre-exponential factor A and the activation enthalpy H^a are substantially anisotropic.

Comparison of the characteristic surfaces of the conductivity tensor in different phases shows that as the temperature is raised and the II-I phase transition is approached the shape of the biaxial ellipsoid in phase II approaches that of the uniaxial ellipsoid typical of the super-ionic phase I, and differs greatly from the shape of biaxial ellipsoid in phase III.

5. ISOTOPIC EFFECT IN CONDUCTIVITY

Comparison of the corresponding components of the conductivity tensor (Fig. 3) and also of the values of A and H^a for CHS and CDS (Table I) in phase I reveals an isotopic effect in conductivity. In particular, the ratio A^H/A^D for various components ranges from 1.3 to 1.5. This agrees well

TABLE I. Parameters H_{ii}^a and A_{ii} describing the temperature dependence of the principal components of the tensor σ_{ij} , and orientation of its principal axes relative to the crystallographic a^* , b , and c^* in the corresponding temperature interval ΔT .

Crystal	Phase	Space group	Component	H_{ii}^a , eV	$\Omega^{-1} \cdot \text{cm}^{-1} \cdot \text{K}$	γ_{ii} , deg	ΔT , K
CsHSO ₄	I	$P2_1/c$	$\begin{cases} \sigma_{11} \\ \sigma_{22} \\ \sigma_{33} \end{cases}$	$\begin{cases} 0,95 \pm 0,05 \\ 0,74 \pm 0,05 \\ 1,05 \pm 0,05 \end{cases}$	$\begin{cases} 3,75 \cdot 10^8 \\ 1,99 \cdot 10^6 \\ 2,19 \cdot 10^9 \end{cases}$	$\begin{cases} 26 \pm 4 \\ 0 \\ 4 \pm 4 \end{cases}$	$\begin{cases} 290-328 \\ 290-328 \\ 290-328 \end{cases}$
			$\begin{cases} \sigma_{11} \\ \sigma_{22} \\ \sigma_{33} \end{cases}$	$\begin{cases} 1,18 \pm 0,05 \\ 1,15 \pm 0,05 \\ 1,55 \pm 0,08 \end{cases}$	$\begin{cases} 1,09 \cdot 10^9 \\ 5,14 \cdot 10^9 \\ 5,44 \cdot 10^{14} \end{cases}$	$\begin{cases} 24 \pm 4 \\ 0 \\ -4 \pm 4 \end{cases}$	$\begin{cases} 333-412 \\ 333-412 \\ 333-412 \end{cases}$
			$\begin{cases} \sigma_{11} \\ \sigma_{22} \\ \sigma_{33} \end{cases}$	$\begin{cases} 0,26 \pm 0,02 \\ 0,26 \pm 0,02 \\ 0,28 \pm 0,02 \end{cases}$	$\begin{cases} 4,36 \cdot 10^3 \\ 4,36 \cdot 10^3 \\ 7,34 \cdot 10^3 \end{cases}$	$\begin{cases} — \\ 0 \\ 0 \end{cases}$	$\begin{cases} 414-470 \\ 414-470 \\ 414-470 \end{cases}$
CsDSO ₄	I	$I4_1/amd$	$\begin{cases} \sigma_{11} \\ \sigma_{22} \\ \sigma_{33} \end{cases}$	$\begin{cases} 0,27 \pm 0,02 \\ 0,27 \pm 0,02 \\ 0,29 \pm 0,02 \end{cases}$	$\begin{cases} 3,5 \cdot 10^3 \\ 3,5 \cdot 10^3 \\ 5,7 \cdot 10^3 \end{cases}$	$\begin{cases} — \\ — \\ 0 \end{cases}$	$\begin{cases} 412-470 \\ 412-470 \\ 412-470 \end{cases}$

with an estimate of this ratio in hopping-conduction theory. Starting with expressions (6) and (10) it is easy to show that

$$A^H/A^D \approx v_0^H/v_0^D \approx (m_D/m_H)^{1/2} \approx 2^{1/2}, \quad (12)$$

where m_D and m_H are the deuteron and proton masses. This indicates that the isotopic effect can be attributed only to a change in the mass of the mobile ions and is not connected with the difference between their quantum-mechanical properties. It should be noted that the authors of an earlier paper¹⁶ observed a significant difference between the conductivities of monoclinic phases of CHS and CDS crystals in the a^* direction, and attributed it to the difference between the tunneling penetrability of the proton and deuteron. They took no account, however, of a number of factors, such as the anisotropy of the conductivity, the different orientations of the crystallographic axes in phases II and III, the contribution of surface component of the conductivity, and also the presence of a III-II structural phase transition having, as noted above, slower kinetics. This last circumstance is also quite important because at temperatures ≈ 400 K, at which the III-II phase transition is practically terminated, the CHS conductivity exceeds that of CDS by only a factor of 2–4 (Fig. 1), and not by the one or two orders of magnitude expected for proton transport by tunneling. The conclusion

of Ref. 16, that the protons tunnel through monoclinic phases of CHS, seems little founded and is most likely wrong. A definite confirmation of the common character of the “classical” mechanism of conductivity in crystals with short ($\approx 2.5-2.6$ Å) hydrogen bonds results from Ref. 17, where it is shown that the isotopic conductivity effect for another protonic conductor CsH₂PO₄ is also described with good accuracy by Eq. (12).

6. EFFECT OF HYDROSTATIC PRESSURE ON PROTON CONDUCTIVITY

The influence of pressure on the ion conductivity is described by the activation volume, which is usually regarded as the change of the crystal volume in the process of formation and migration of a mobile defect.¹⁷ We shall show below, however, that in view of the specific character of hydrogen bonds the variation of the potential relief with pressure may turn out to be more substantial. The expression for the activation volume in terms of the measurable experimental parameters of the ion conductivity follows from the thermodynamic relation

$$V = \left(\frac{d\Phi}{dp} \right)_T \quad (13)$$

and from Eqs. (9) and (10). As a result,

$$V^a(\mathbf{n}) = -T \left[\left(\frac{\partial \ln \sigma(\mathbf{n})}{\partial p} \right)_T + \left(\frac{\partial \ln A(\mathbf{n})}{\partial p} \right)_T \right] \quad (14)$$

It follows from this equation that to calculate $V^a(\mathbf{n})$ it is necessary in general to know both the isothermal $[\sigma(p)]$ at constant T and the isobaric $[\sigma(T)]$ at constant p dependences of the ion conductivity. These most typical dependences are shown for CHS and CDS in Figs. 3–5. Analysis of the isobaric dependences shows that the change of the pre-exponential factor in Eq. (10) and the derivatives $\partial \ln A / \partial p$ calculated from this change do not exceed the experimental error and are less than $\pm 3 \cdot 10^{-12} \text{ cm}^2/\text{dyn}$. Approximately the same values are obtained from calculations of $\partial \ln A / \partial p$ based on continuum models of diffusion¹⁸ and ionic conductivity.¹⁹ In fact, according to Ref. 19 the second term in the right-hand side of (14) can be expressed in terms of the Grüneisen parameter γ and the bulk compressibility α :

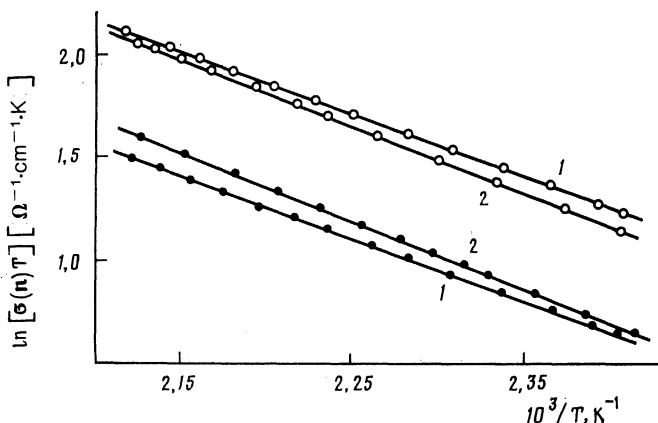


FIG. 3. Dependence of $\ln [\sigma(\mathbf{n})T]$ on $1/T$, measured perpendicular and parallel to the tetragonal axis in superionic phases of the crystals CsHSO₄ (○) and CsDSO₄ (●): 1— σ_1 ; 2— σ_{\parallel} .

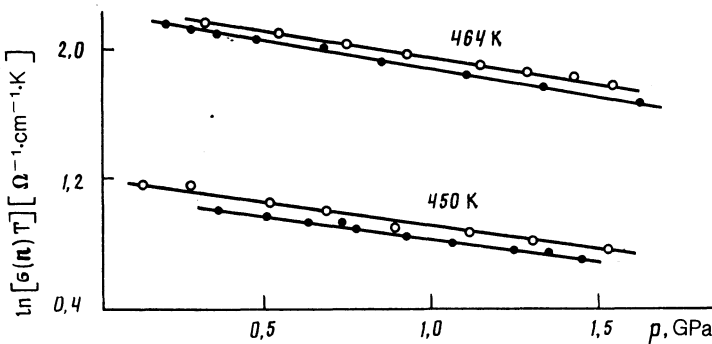


FIG. 4. Baric dependence of $\ln[\sigma(n)T]$ in the super-ionic phase of the crystal CsHSO_4 along and across the tetragonal axis at various temperatures: \circ — σ_1 ; \bullet — σ_2 .

$$(\partial \ln A / \partial p)_T = \kappa (\gamma - 2/3). \quad (15)$$

In the case of an isotropic solid we have

$$\gamma = \alpha V_M / \kappa c_V \approx \alpha V_M / \kappa c_p, \quad (16)$$

where α is the bulk coefficient of thermal expansion, V_M is the moar volume, and c_V and c_p are the specific heats at constant volume and pressure.

Substituting in (15) and (16) the experimental values for CHS in phase III ($\alpha = 1.3 \cdot 10^{-4} \text{ deg}^{-1}$ [Ref. 20]; $V_M = 67 \text{ cm}^3/\text{mol}$ [Ref. 21], $\kappa = 3.3 \cdot 10^{-12} \text{ cm}^2/\text{dyn}$, $c_p = 1.4 \cdot 10^9 \text{ erg/mol.deg}$ at $T = 300 \text{ K}$ [Ref. 22]), and for the super-ionic phase I ($\alpha = 1.7 \cdot 10^{-4} \text{ deg}^{-1}$ [Ref. 20], $V_M = 69 \text{ cm}^3/\text{mol}$ [Ref. 7], $\kappa = 6.3 \cdot 10^{-12} \text{ cm}^2/\text{dyn}$ and $c_p = 1.4 \cdot 10^9 \text{ erg/mol.deg}$ at $T = 510 \text{ K}$ [Ref. 22]), we find that in the temperature interval 300–510 K the values of $\partial \ln A / \partial p$ vary in the range $6.4 \cdot 10^{-12} - 3.8 \cdot 10^{-12} \text{ cm}^2/\text{dyn}$. The corresponding corrections to the activation volume in this temperature interval, to account for the second term in the right-hand side of (14), amount to $0.22 - 0.26 \text{ cm}^3/\text{mol}$. Similar estimates are obtained for phase II. It can therefore be concluded that neglect of the second term in the right-hand side of (14) can lead to an activation-volume error of at most $0.3 \text{ cm}^3/\text{mol}$.

It follows from the isobaric and isothermal dependence of the conductivity (Figs. 4–6) that pressure exerts substantially different influences on the proton conductivity in different phases. In the super-ionic phase I, the conductivity decreases linearly with pressure both along and across the

tetragonal axis (Fig. 4). From the orientation of the conductivity tensor in phase II one should expect significant differences in the character of the $\sigma(p)$ dependence in the a^* and c^* directions. The measurements show, however, that the conductivities in both directions are independent of pressure within the limits of experimental error (Fig. 5). In phase III the pressure has qualitatively different effects on the conductivities in different crystallographic directions: $\sigma(b)$ increases and $\sigma(a^*)$ decreases when the pressure is raised to $p = 0.75 \text{ GPa}$ (Fig. 6). For $p \geq 0.75 \text{ GPa}$, however, the form of $\sigma(b) = f(p)$ changes fundamentally (Fig. 6)—the conductivity decreases with pressure. Unfortunately, investigation of its baric dependence was made impossible by the low values of the conductivity $\sigma(c^*)$. For the same reason it was also difficult to investigate $\sigma(a^*) = f(p)$ at $\leq 310 \text{ K}$.

Table II lists the activation volumes calculated from the isothermal dependence of the conductivity using Eq. (14) with the term $\partial \ln A / \partial p$ neglected. The activation volume of the proton conductivity is a structure-sensitive parameter and ranges from -2 to $2 \text{ cm}^3/\text{mol}$, depending on the structural features of the phases.

As seen from Fig. 6, a distinguishing feature of the $\sigma = f(p)$ dependences at temperatures corresponding to phase III ($T < 330 \text{ K}$) is also an abrupt change of σ in the immediate vicinity of $p \approx 0.75 \text{ GPa}$. No pressure hysteresis is observed within the limits of experimental error. It is noteworthy that the conductivity baric plots measured at 1 kHz agree with analogous dependences measured with direct current, thereby excluding a possible contribution of

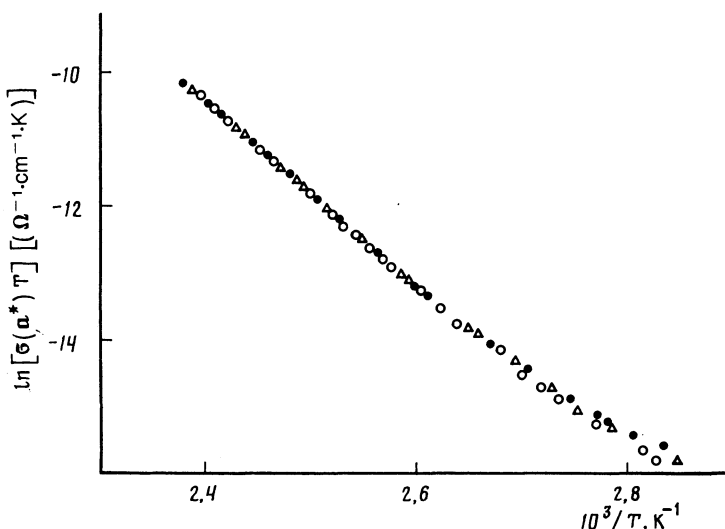


FIG. 5. Temperature dependence of the conductivity $\sigma(a^*)$ in phase II of CsDSO_4 crystal at various hydrostatic pressures: \bullet — 0.3 GPa ; Δ — 0.6 GPa ; \circ — 0.9 GPa .

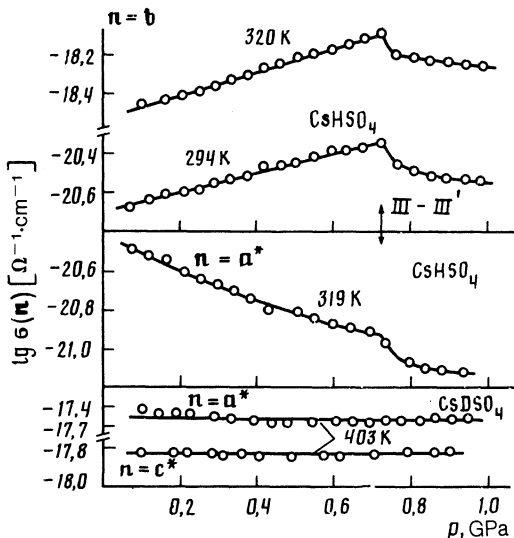


FIG. 6. Baric dependence of conductivity in phases III and II. The arrows point to the III-III' phase transition in CsHSO_4 crystal (see the text).

some low-frequency relaxation processes to the measurable conductivity.

Anomalies at $p = 0.75$ GPa were observed also on the baric plots of the dielectric constant ϵ_n . It follows from Fig. 7, however, that these anomalies differ qualitatively in form from the conductivity anomalies. The kink anomalies on the plots of ϵ vs. temperature are known to correspond to second-order structural phase transitions. It can therefore be assumed that in this case the anomalies on the baric plots of σ and ϵ attest to a baric second-order structural phase transition from phase III into a new phase III' realized at a pressure $p > 0.75$ GPa.

7. DISCUSSION OF RESULTS

Our results lead to a specific application of the theory developed in Sec. 3 for hopping conductivity to the crystals CHS and CDS. It follows from Eq. (8) that the temperature dependence of the conductivity tensor is described in general by a sum of exponentials. Nonetheless, calculations of the temperature dependence of the principal components of the conductivity tensor in each of the phases of CHS and CDS show that this dependence is simpler and is well described by only a single exponential such as (10). This suggests that one can distinguish along these lines (in a corresponding

temperature interval) proton sites of a type such that a proton hop between them is indeed decisive for transport processes in a given direction.

According to structural investigations,^{7,10} in the super-ionic phase I of CHS (CDS) the four protons per unit cell are distributed among locations belonging to at least two different crystallographic positions corresponding to the H-bond center: eightfold (*e*) and sixteenfold (*f*).

It was shown in Ref. 23 that in phase I protons migrating only over positions of type *e* or only over positions of type *f* produce two-dimensional conductivity in the (001) plane. The necessary condition for realization of three-dimensional conductivity is the presence of hops between positions of types *e* and *f*. Only then will the protons have connected diffusion paths along the *c* axis. The corresponding expressions obtained for the components σ_1 and σ_{\parallel} on the basis of Eq. (6) call for a detailed analysis.

The derivation of appropriate expressions for the conductivity tensor is in this case considerably more complicated and is a separate problem. However, qualitative estimates of the thermodynamic parameters that characterize the proton conductivity can be obtained from Eqs. (7)-(10) by expressing the pre-exponential factor in the form

$$A(\mathbf{n}) = \frac{1}{2} \frac{n_0(eZ)^2}{k_B} v_0(\mathbf{n}) l^2(\mathbf{n}) \exp\left[\frac{S(\mathbf{n})}{k_B}\right], \quad (17)$$

where $S(\mathbf{n})$ is the effective change of the entropy in photon migration along \mathbf{n} ; $v_0(\mathbf{n})$ and $l(\mathbf{n})$ are the oscillation frequency and the hopping length in the \mathbf{n} direction; n_0 is the density of the mobile carriers. Let us estimate $S(\mathbf{n})$, which coincides for the super-ionic phase with the migration entropy S_n . Substituting in (17) $n_0 \approx 9 \cdot 10^{21} \text{ cm}^{-3}$ (Refs. 7 and 10), $v_0 \approx 3 \cdot 10^{13} \text{ s}^{-1}$ (Ref. 25), $l \approx 10^{-8} \text{ cm}$ (Refs. 7 and 10), and the experimental values of $A(\mathbf{n})$ we obtain $S_m \approx (1-2) k_B$.

We have already noted that the structure of the monoclinic phase II can be regarded as a weak distortion of the structure of the tetragonal (super-ionic) phase I (Refs. 7 and 9). In the phase transition I-II the total number of positions accessible to protons is therefore unchanged, but each (*e* and *f*) position of the tetragonal phase the change to the monoclinic phase splits into several positions of lower multiplicity. Since the four protons per unit cell of the monoclinic phase occupy only one fourfold position, the usual static network of hydrogen bonds is realized in this phase, while

TABLE II. Pre-exponential factor $A(\mathbf{n})$, of the activation enthalpy $H^a(\mathbf{n})$ in the corresponding temperature interval ΔT and in the activation volume $V^a(\mathbf{n})$ for certain crystallographic directions.

Crystal	Phase	Orientation	$A(\mathbf{n})$, $\Omega^{-1} \cdot \text{cm}^{-1} \cdot \text{K}$	$H^a(\mathbf{n})$, eV	ΔT , K	$V^a(\mathbf{n})$, cm^3/mol
CsHSO_4	{III}	{a *}	$3,80 \cdot 10^8$	$0,94 \pm 0,02$	290-328	$2,0 \pm 0,3$
		b	$1,68 \cdot 10^6$	$0,76 \pm 0,02$	290-328	$-1,6 \pm 0,3$
CsDSO_4	II	a *	$5,28 \cdot 10^6$	$0,76 \pm 0,02$	290-328	$1,4 \pm 0,3$
CsHSO_4	I	a	$4,83 \cdot 10^{10}$	$1,21 \pm 0,03$	315-412	$\pm 0,3^2$
		c *	$2,05 \cdot 10^{13}$	$1,47 \pm 0,05$	350-412	$\pm 0,3$
		c	$4,36 \cdot 10^3$	$0,26 \pm 0,02$	414-470	$0,9 \pm 0,3$
		e	$7,34 \cdot 10^3$	$0,28 \pm 0,02$	414-470	$1,2 \pm 0,3$

¹High-pressure phase realized at $p > 0.75$ GPa (see the text). The orientation of the **b** axis corresponds to phase III.

² $V^a(\mathbf{n}) = 0$ within the limits of the indicated experimental error.

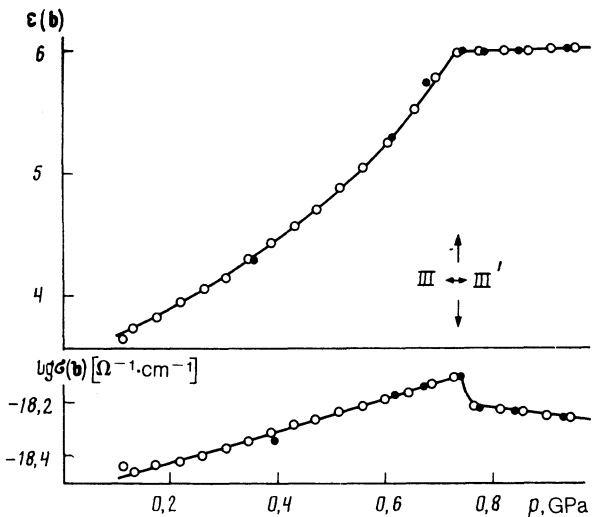


FIG. 7. Baric dependence of the dielectric constant $\epsilon(b)$ and the conductivity $\sigma(b)$ in CsHSO_4 crystal at $T = 320$ K in the vicinity of a III-III' phase transition. ○—Increasing pressure; ●—decreasing pressure.

the proton conductivity results only from proton defects, viz., protons forming weak hydrogen bonds in interstices, and proton vacancies in sites. In the case of intrinsic defects, the proton density n_q in each system of interstitial positions is given by

$$n_q = \left(\frac{g_q}{g_0} \right)^{\nu_2} n_0 \exp \left(-\frac{\Phi_q^f}{2k_B T} \right), \quad (18)$$

where Φ_q^f is the thermodynamic potential of defect formation for positions of type q . The entropy $S(n)$ in expression (17) for low-conductivity phases will include two terms: the migration entropy S_m and the formation entropy S_f for the corresponding type of ion defect. It is important that the parameters $\nu_0(n)$ and $l(n)$ in the pre-exponential factor of (17) are practically the same in phase II as in phase I. Therefore the large experimental values of $A(n)$ in phase II compared with the super-ionic phase I (Table I) are due mainly to the factor $\exp(S_f/k_B)$, where S_f is the entropy of formation of the proton defect. The directions of the principal axes of the conductivity tensor, obtained by calculating S_f using Eq. (17) and the experimental values of $A(n)$ yield values $S_f/k_B \approx 10-15$, considerably higher than the activation entropy in the super-ionic phase. This result agrees with the theoretical estimates of Ref. 14, which indicate that the entropy of defect formation is considerably larger than the entropy of defect migration.

Taking into account the similarity of the structures of phases III and II, we can expect the mechanism of the proton conductivity in the monoclinic phase III to be similar to that considered above. A quantitative description, however, requires a detailed symmetry analysis of the I-III phase transition.

Our experimental data (Table II) show that the activation volume is a more structure-sensitive parameter than the activation energy and the pre-exponential factor in Eq. (10) (Table II). This is most clearly manifested in the III-III' phase transition, when $H^a(b)$ and $A(b)$ remain practically unchanged, while $V^0(b)$ reverses sign.

For crystals with metal-ion conductivity (such as

NaCl) the activation volume for defect formation and migrations are described satisfactorily by the hard-sphere model, with the sphere radii corresponding to crystal-chemical radii of the ions. According to this model, the activation volume of proton conductors should be zero, since the H^+ ion radius is zero. However, as seen from our present investigations (Table II), the proton-conductivity activation volume varies over a rather wide range and can be positive as well as negative. In addition, proton migration in crystals with hydrogen bonds has a specific singularity that complicates the microscopic interpretation of the experimentally obtained quantity $V^a(n)$. It was assumed above in the analysis of the conductivity anisotropy that the protons occupy a position at the center of the H-bonds. Actually, since in all CHS and CDS phases the H-bond lengths exceed 2.5 Å (Refs. 5, 7, 10), the potential of the hydrogen atom of such H bonds is characterized by two minima,^{26,27} i.e., they are non-central. Accordingly, the proton-transport mechanism should in this case be similar to the Grotthuss mechanism² and include two obligatory stages: 1—proton transport between two positions on an H bond; 2—breaking of the H bond with the oxygen acceptor atom, accompanied by reorientation of the O-H or SO_4-H complex and formation of a new hydrogen bond with a neighboring oxygen acceptor atom. It should be noted that in the analysis of the conductivity anisotropy allowance for the noncentral location of the proton on the H bond is immaterial, but to interpret the results on the influence of pressure on proton conductivity this circumstance may turn out to be quite important. From the phenomenological point of view, the measured activation volume is determined by two factors:

1) Formation and migration of proton defects, just as in classical ion conductors, is accompanied by a change of the crystal volume, while the appearance of a term $pV_{\text{geom}}^a(n)$ in the exponential of (10) is due to the fact that at higher pressure more work is done against the external forces.

2) The hydrogen-bond length varies with pressure, which changes the energy of this band and hence also the conductivity activation energy. In accordance with the mechanism of two-stage transport of the proton, we can write for this case

$$V_{\text{en}}^a = \partial E^a / \partial p \approx \partial E_1 / \partial p + \partial E_2 / \partial p = (\partial E_1 / \partial R + \partial E_2 / \partial R) (\partial R / \partial p), \quad (19)$$

where E_1 is the barrier between two minima on the H bond, E_2 is the hydrogen-bond breaking energy, and R is the bond length. From the experimental data²⁷ and the theory of the hydrogen bond²⁸ it follows that E_2 is a decreasing function and E_1 an increasing function of R . Therefore their derivatives in (23) will make contributions of opposite sign. It is possible that the competition of these contributions will in fact give rise to the experimentally observed changes of V^a in the range from -1.6 to $2 \text{ cm}^3/\text{mol}$.

In conclusion, the authors thank N. M. Shchagina and V. A. Dolbinina for supplying the crystals, and also B. V. Marinov and R. A. Dilanyan for a helpful discussion of the results.

¹ Shubnikov Crystallography Institute, USSR Academy of Sciences

² L. Glasser, Chem. Rev. **75**, 21 (1975).

³ S. Chandra, Materials Sci. Forum **1**, 153 (1984).

⁴ A. I. Baranov, Izv. AN SSSR ser. fiz. **51**, 2146 (1987).

- ⁴A. I. Baranov, L. A. Shuvalov, and N. M. Shagin, Pis'ma Zh. Eksp. Teor. Fiz. **36**, 381 (1982) [JETP Lett. **36**, 459 (1982)].
- ⁵V. B. Merinov, A. N. Baranov, B. A. Maksimov, and L. A. Shuvalov, Kristallografiya **31**, 450 (1986) [Sov. Crystallography **31**, 264 (1986)].
- ⁶A. M. Balagurov, A. V. Belushkin, A. I. Beskrovnyi *et al.*, Krat. Soobshch. Fiz. FIAN No. 13, p. 18 (1985).
- ⁷B. M. Merinov, A. I. Baranov, L. A. Shuvalov, and B. A. Maksimov, Kristallografiya, **32**, 86 (1987) [Sov. Phys. Crystallography **32**, 47 (1987)].
- ⁸A. I. Baranov, L. A. Shuvalov, and N. M. Shchagina, *ibid.* **29**, 1203 (1984) [Sov. Phys. Crystallography **29**, 706 (1984)].
- ⁹N. A. Dzhavadov, Soobshcheniya OIYaI, R17-80-248 (1985).
- ¹⁰A. V. Belushkin, L. A. Shuvalov, V. I. David, and R. M. Ibberson, *ibid.* E14-90-272 (1990).
- ¹¹R. Blinc, J. Dolinsek, G. Lahainar *et al.*, Phys. Stat. Sol. **123**, k84 (1986).
- ¹²A. I. Baranov, V. V. Sinitsyn, E. T. Ponyatovskii, and L. A. Shuvalov, Pis'ma Zh. Eksp. Teor. Fiz. **44**, 186 (1986) [JETP Lett. **44**, 237 (1986)].
- ¹³A. V. Tregubchenko, Candidate's dissertation, Crystallography Inst. USSR Acad. Sci., 1988.
- ¹⁴C. P. Flynn, *Point Defect and Diffusion*, Clarendon, Oxford, 1972.
- ¹⁵A. I. Baranov and A. V. Tregubchenko, Izv. AN SSSR ser. fiz., **53**, 1394 (1989).
- ¹⁶I. G. Khaïnovskii, Yu. T. Pavlyukhin, and Z. F. Khaïretdinov, Izv. SO AN SSSR, Ser. Khim. Nauk **11**, 99 (1985).
- ¹⁷A. N. Baranov, V. P. Khiznichenko, and L. A. Shuvalov, Abstracts, 9th All-Union Conf. on Phys. Chemistry and Electrochemistry of Ionic Melts and Solid Electrolytes (Sverdlovsk, 1987), Vol. 3, p. 225.
- ¹⁸R. Keiss, in *Solids Under Pressure*, V. Paul and D. Warschauer, eds., McGraw, 1963.
- ¹⁹G. A. Samara, Sol. St. Phys. **38**, 1 (1984).
- ²⁰R. A. Dilanyan, Cand. Dissert., Inst. Solid State Phys., 1989.
- ²¹K. Itoh, T. Ozaki, and E. Nakamura, Acta Cryst. B **37**, 1908 (1981).
- ²²M. Kamikae, T. Osakam, Y. Makita *et al.*, J. Phys. Soc. Jpn. **50**, 3167 (1981).
- ²³A. P. Levanyuk and D. G. Sannikov, Zh. Eksp. Teor. Fiz. **55**, 256 (1968) [Sov. Phys. JETP **27**, 134 (1969)].
- ²⁴A. I. Baranov, B. V. Merinov, A. V. Tregubchenko *et al.*, Sol. St. Ionics, **36**, 279 (1989).
- ²⁵V. P. Dmitriev, V. V. Loshkarev, L. M. Rabkin *et al.*, Kristallografiya **31**, 1138 (1986) [Sov. Phys. Crystallography **31**, 673 (1986)].
- ²⁶J. D. Brown, Acta Cryst. A **32**, 24 (1976).
- ²⁷M. Ichikawa, *ibid.* B **34**, 2074 (1978).
- ²⁸E. R. Lippincott and R. Schroeder, J. Chem. Phys. **23**, 1099 (1955).

Translated by J. G. Adashko